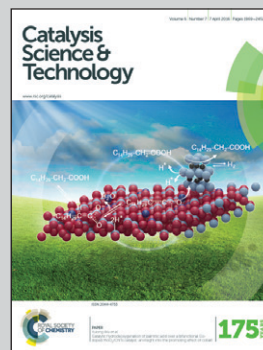


Showcasing research from Dr. Jung Inn Sohn's group at the University of Oxford, United Kingdom, and Prof. Kyung-Won Park's group at Soongsil University, Republic of Korea

Title: Synergistic incorporation of hybrid heterobimetal–nitrogen atoms into carbon structures for superior oxygen electroreduction performance

As a promising alternative electrode to Pt-based catalysts for the oxygen reduction reaction (ORR) in PEMFCs, the hybrid-functional carbon nanostructures, with a high content of non-precious heterobimetal–nitrogen atoms synthesized by a modified electrospinning technique, exhibit remarkably superior ORR electrocatalytic properties due to their unique doping structures and modified electric structures.

As featured in:



See Kyung-Won Park, Jung Inn Sohn *et al.* *Catal. Sci. Technol.*, 2016, 6, 2085.



www.rsc.org/catalysis

Registered charity number: 207890

Cite this: *Catal. Sci. Technol.*, 2016,
6, 2085

Synergistic incorporation of hybrid heterobimetal–nitrogen atoms into carbon structures for superior oxygen electroreduction performance†

Young-Woo Lee,^a Geon-Hyoung An,^b Seul Lee,^c John Hong,^a Byung-Sung Kim,^a
Juwon Lee,^a Da-Hee Kwak,^c Hyo-Jin Ahn,^b Wansoo Huh,^c Seung Nam Cha,^a
Kyung-Won Park,^{*c} Jung Inn Sohn^{*a} and Jong Min Kim^a

Although Pt-based catalytic technology has led to significant advances in the development of electrocatalysts in fuel cells, Pt replacement with efficient and stable non-precious metal catalysts has a great technological significance for successful large-scale implementation of fuel cells. Here, we present the development of hybrid functional 1-dimensional carbon structures incorporated homogeneously with high contents of non-precious metal multi-dopants, consisting of iron, cobalt and nitrogen, as a promising alternative to Pt-based catalysts for the cathodic oxygen reduction reaction (ORR) through a modified electrospinning technique. These hybrid heterobimetal–nitrogen-incorporated carbon structures exhibit superior ORR electrocatalytic properties *i.e.*, more positive reduction potential, high electroreduction current density, high electron transfer value (~ 3.87) close to the perfect ORR and improved electrochemical stability with a very small decrease of ~ 8 mV in half-wave potential. The observed enhancement in electrochemical performance can be ascribed to the increased amount of catalytically active sites with relatively high contents of heterometallic iron and cobalt atoms surrounded by nitrogen species and their homogeneous distribution on the catalyst surface.

Received 24th November 2015,
Accepted 27th December 2015

DOI: 10.1039/c5cy02016f

www.rsc.org/catalysis

Introduction

Since the successful demonstration of the earliest concept of a fuel cell in the nineteenth century, the polymer electrolyte membrane fuel cell (PEMFC) has been represented as one of the most promising alternative energy conversion technologies available today for the production of high power density at relatively low operating temperature and low environmental impact of producing energy from nonpolluting and renewable energy sources for electric vehicles and portable electronic devices.^{1–3} However, in spite of significant progress being made to improve the availability of PEMFC technologies for extension to large-scale applications over the past decade, the actual implementation of sustainable development continues to face various challenges, such as the manufacturing cost

and the long-term durability and performance. Particularly, the development of highly efficient, stable and low-cost catalysts, preferably free of precious noble metals, has been arguably considered as the most important and innovative challenge for the successful large-scale commercial production of PEMFCs.^{4,5}

To date, it has been demonstrated that platinum (Pt) exhibits the most efficient electrocatalytic activity at both electrodes of PEMFCs even though its prohibitive cost and scarcity have hindered the widespread utilization of PEMFCs.^{6–10} Furthermore, the oxygen reduction reaction (ORR) at the cathode, requiring comparatively much more Pt, plays a key role in determining the performance of a fuel cell because of the sluggish ORR kinetics compared to the fast hydrogen oxidation kinetics at the anode.^{11–14} In this regard, Pt replacement through the development of non-precious metal catalysts with high ORR activity and good stability becomes of practical importance in meeting the demand for ultimately affordable, scalable and eco-friendly technologies. For this reason, enormous research efforts have been devoted to the development of new ORR catalysts as alternatives to Pt or Pt-based catalysts, including various transition metal complexes^{15,16} and carbon-based materials doped with non-metallic elements.¹⁷ Among the diverse non-precious metal electrocatalysts studied to date, carbon-supported structures,

^a Department of Engineering Science, University of Oxford, Oxford OX1 3PJ, UK.E-mail: junginn.sohn@eng.ox.ac.uk; Fax: +44 (0)1865 273010;

Tel: +44 (0)1865 273912

^b Department of Materials Science and Engineering, Seoul National University of Science and Technology, Seoul 139-743, Republic of Korea^c Department of Chemical Engineering, Soongsil University, Seoul 156-743, Republic of Korea. E-mail: kwpark@ssu.ac.kr; Fax: +82 2 812 5378;

Tel: +82 2 820 0613

† Electronic supplementary information (ESI) available. See DOI: 10.1039/c5cy02016f

such as carbon nanotubes,¹⁸ graphene/reduced graphene oxides,^{19,20} carbon nanofibers²¹ and mesoporous carbon,²² have attracted great attention because of their low cost, environmental friendliness and infinite natural resources. Moreover, it has been recently demonstrated that carbon-based catalysts doped with nitrogen and transition metal–nitrogen for the ORR have shown high electrochemical activity and stability.^{23–27} Very recently, various macrocyclic transition-metal ($M-N_x$) carbon-based compounds with promising ORR electrocatalytic activity have been extensively studied to achieve high ORR performance, although there have been continued debates on the nature of ORR mechanisms associated with active catalytic sites in such $M-N_x$ structures.^{17,28} However, despite the highly selective electrocatalytic activity of the $M-N_x$ carbon-based nanostructures as non-precious metal catalysts, a conventional synthetic approach usually requires complex or multi-step processing techniques as well as high temperature annealing processes to prepare carbon-based catalysts doped or co-doped with nitrogen and/or transition metals.^{25,29–32} Apart from complicated multi-processes for doping, these synthetic methods also suffer from several problems, such as the compositional non-homogeneity of doping elements, low contents of dopants on the catalyst surface, and the partial presence of aggregated metallic or metal-based compound phases.^{33–35}

In this work, we introduce a facile method to design and synthesize efficiently functionalized carbon structures incorporated homogeneously with heterobimetallic dopants

serving as active sites on the catalyst surface for superior electrochemical activity in ORRs. Furthermore, we propose a hybrid heterobimetal–nitrogen-doped carbon structure (denoted as HDCS) as an efficient ORR electrocatalyst in PEMFCs, synthesized using a simple electrospinning method with polyacrylonitrile (PAN) as a carbon source and metal–phtalocyanine ($M-Pc$, $M = Fe$ and Co) comprising nitrogen and transition metal elements as hybrid dopant sources. These obtained HDCSs present high contents of transition metal and nitrogen atoms homogeneously distributed on the catalyst surface, and hence exhibit superior ORR activity and excellent electrochemical stability comparable to those of commercial Pt electrocatalysts.

Results and discussion

Fig. 1(a) shows the schematic illustration of the sequential steps for the synthesis of HDCSs. In the first step, the as-electrospun 1-dimensional (1-D) fibers were prepared using PAN as a carbon source and $M-Pc$ consisting of both $Fe-Pc$ and $Co-Pc$ as the heterometal and nitrogen doping sources. The as-electrospun fibers were dried in an oven at 60 °C for 24 h and then pyrolyzed in a tube furnace at 900 °C for 3 h under a nitrogen atmosphere to finally obtain the HDCSs. Additionally, various HDCSs with different doping concentrations were also synthesized by controlling the weight fractions of $M-Pc$ precursors in an electrospun solution in the range of low (1 wt%: HDCS-L), middle (5 wt%: HDCS-M) and

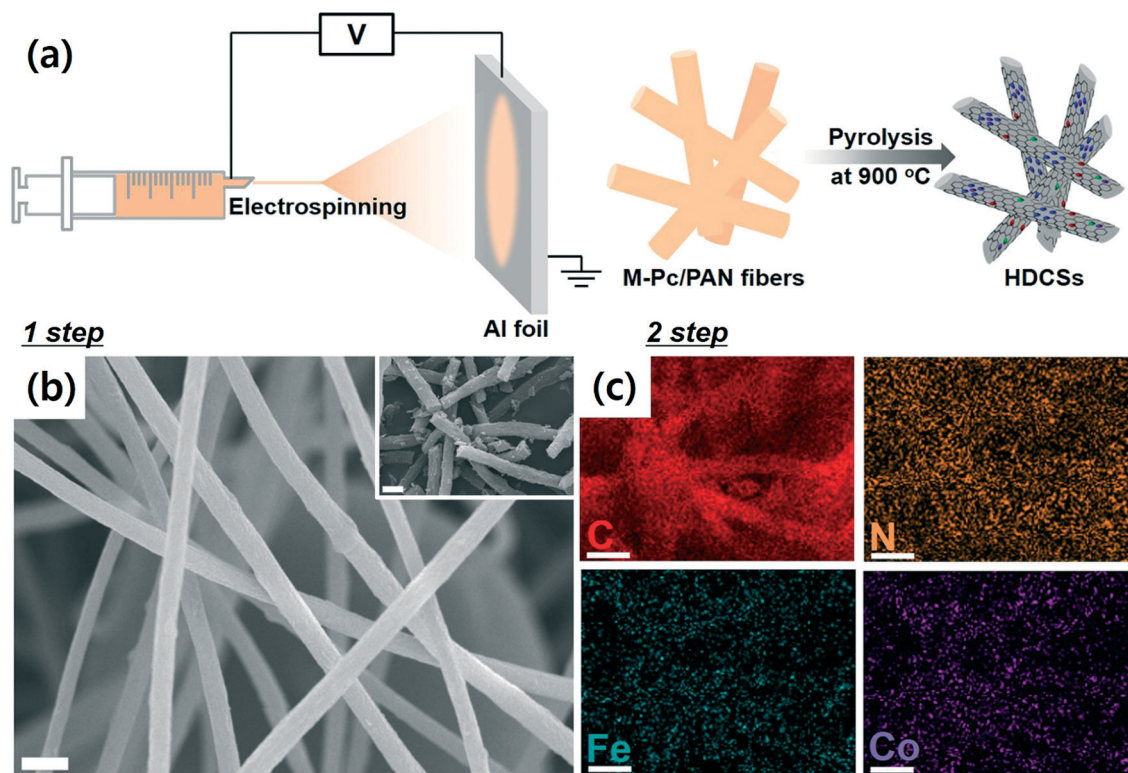


Fig. 1 (a) Schematic illustration of the synthesis process of the HDCSs. (b) SEM image of the as-prepared HDCS-H. (c) EDX element mapping images for C, N, Fe and Co of HDCS-H indicated in the inset of Fig. 1(b). The scale bar of Fig. 1(b and c) is 2 μ m.

high (10 wt%: HDCS-H) fractions. The morphology of the HDCSs was investigated by field-emission scanning electron microscopy (FE-SEM) and field-emission transmission electron microscopy (FE-TEM). As shown in the FE-SEM and FE-TEM images (see the insert) in Fig. S1(a-c),† the HDCSs with a 1-D structure were well formed and their diameters were approximately 0.8–1.2 μm . Here, note that all the as-prepared HDCSs have similar diameters regardless of the doping precursor fractions as shown in Fig. S1(a-c).† We also clearly observed that the HDCSs have amorphous carbon structures as seen in the XRD patterns (Fig. S1(d)†). However, no crystal peaks, such as those for any metallic and metal-based compound phases, were observed in all HDCSs.

In order to further assess the elemental compositions and distributions of the hybrid dopants in the HDCSs, energy-dispersive X-ray (EDX) examinations were carried out. Fig. 1(c) shows the elemental mapping of carbon, nitrogen, iron and cobalt elements, which were uniformly distributed on the 1-D carbon fibers. In particular, it is evident that the metal elements such as Fe and Co were incorporated with carbon and nitrogen species in the structures. These are consistent with the XRD results in Fig. S1(d)† showing no unwanted metallic or metal-based compounds, that is, good incorporation of dopants into the carbon structures.

The chemical structure and quantity of doping elements acting as electrochemically active sites on the catalyst surface would be another key factor greatly affecting the ORR performance. Therefore, to determine the chemical state and content of transition metals and nitrogen in the HDCSs, we performed XPS measurements. As shown in Fig. 2(a), the Co 2p XPS spectra of the as-prepared HDCSs consist of Co 2p_{3/2} at ~ 781.6 eV and Co 2p_{1/2} at ~ 796.8 eV. The peaks of Co 2p_{3/2} located around 779.6, 781.0 and 784.7 eV are assigned to the oxidized Co phase, Co–N bond and satellite, respectively.^{36–39} Moreover, as expected, as the doping precursor fractions increase, the amount of cobalt element increases in the HDCSs, that is, 0.24 for HDCS-L, 0.34 for HDCS-M and 0.47 at% for HDCS-H. Similar to the Co 2p XPS spectra, we found that the Fe 2p_{3/2} spectra of the as-prepared HDCSs consist of oxidized states of Fe with binding energies of 710.9, 712.8 and 716.0 eV, corresponding to Fe–N, Fe³⁺ and satellite, respectively,^{40,41} as shown in Fig. 2(b). It was also observed that the Fe contents of the as-prepared HDCSs increase with increasing fraction of the M-Pc precursors as hybrid doping sources and are 0.22, 0.25 and 0.31 at% for HDCS-L, HDCS-M and HDCS-H, respectively. We summarized the ratio of the doped Fe, Co and N elements as shown in Table 1. In addition, noticeably, the presence of structural

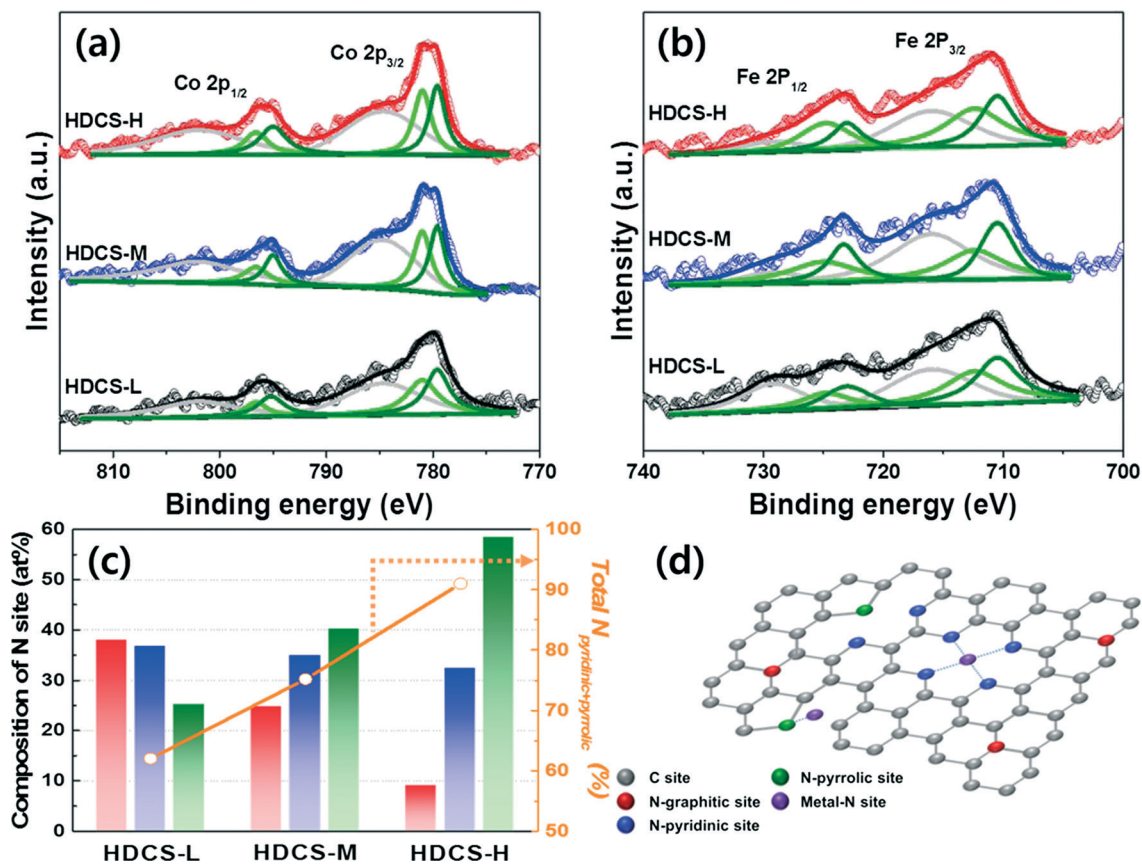


Fig. 2 (a) Co 2p and (b) Fe 2p XPS spectra of the as-prepared HDCSs. (c) Composition of N species of the as-prepared HDCSs. (d) Schematic illustration of representative N and metal doping sites in the carbon structures.

Table 1 Ratio of the doped N, Fe and Co elements in the as-prepared HDCSs obtained from the XPS analysis

	N	Fe	Co
HDCS-L	2.43 at%	0.22 at%	0.24 at%
HDCS-M	4.64 at%	0.25 at%	0.34 at%
HDCS-H	4.42 at%	0.31 at%	0.47 at%

nitrogen in the HDCSs was confirmed by the high-resolution N 1s spectra, showing the incorporation of pyridinic-N (398 eV), pyrrolic-N (400.5 eV) and graphitic-N (401.5 eV) atoms into the carbon structure,^{42,43} as shown in Fig. S2.† Interestingly, as shown in Fig. 2(c), it was found that the total nitrogen contents related to both pyridinic-N and pyrrolic-N sites increase, but the amount of graphitic-N sites decrease as the hybrid doping precursor fractions increase. Here, it is important to note that the pyridinic-N and pyrrolic-N sites are energetically more favorable to bind with metal atoms compared to graphitic-N sites,⁴⁴ as shown in Fig. 2(d). We also note that the relatively higher heterometal dopant contents are observed in the HDCS-H sample. Thus, these indicate that a significant increase in both metal and nitrogen contents is associated with the synergistic incorporation and distribution of dopants into the carbon structures as a result of the presence of M-Pc involving ternary heteroatom dopants (Co, Fe, N). Consequently, it is expected that the modified HDCS through the incorporation of hybrid metal and nitrogen dopants, acting as active sites, can improve the electrochemical activity in ORRs.

To identify the electrochemical activities of the HDCS electrocatalysts in ORRs, cyclic voltammogram (CV) examinations were carried out in Ar- and O₂-saturated 1.0 M KOH solutions between -0.9 and +0.3 V (vs. Hg/HgO). As shown in Fig. 3(a), all the as-prepared HDCS electrocatalysts exhibited a large cathodic peak around -0.1 V in the O₂-saturated electrolyte, whereas no obvious response peak was observed in the Ar-saturated electrolyte. This result suggests that the HDCS can be used as a potential electrocatalyst for the ORR. Furthermore, it was also observed that the oxygen reduction

potentials of the HDCS-H (0.035 V) samples were shifted toward the positive potential direction compared with those of the HDCS-M (0.026 V) and HDCS-L (0.001 V) samples and their maximum current density in the O₂-saturated electrolyte was much greater than those of the HDCS-M and HDCS-L samples. These findings indicate that the ORR activity of the HDCS-H electrocatalyst is superior to those of the HDCS-M and HDCS-L electrocatalysts as a result of the hybrid hetero-transition metal–nitrogen–carbon catalytic systems with large contents of active sites, as shown in Fig. 3(b).

To examine further the ORR activity of the obtained HDCS electrocatalysts, we performed linear sweep voltammetry (LSV) measurements in an O₂-saturated 1.0 M KOH electrolyte at various rotation speeds ranging from 100 to 2500 rpm. For comparison, commercial Pt/C electrocatalysts (E-TEK Co.) were used. As shown in Fig. 4(a) and S3,† the current density (3.44 mA cm⁻²) of the HDCS-H electrocatalyst is considerably higher than that of the HDCS-M (2.37 mA cm⁻²) and HDCS-L (0.98 mA cm⁻²) electrocatalysts at a high potential of 0.04 V and a rotation speed of 1600 rpm, which is comparable to that of a commercial Pt/C electrocatalyst. Additionally, the HDCS-H electrocatalyst (0.07 V) exhibited a more positive half-wave potential in comparison with the HDCS-M (0.04 V) and HDCS-L (0.02 V) electrocatalysts. Also, in order to address whether the HDCS catalysts enable the achievement of a complete reduction reaction of oxygen followed by four electron transfer processes, we calculated the electron transfer numbers of the electrocatalysts based on the slope of the Koutecky–Levich equation as follows:

$$\frac{1}{j} = \frac{1}{j_k} + \frac{1}{B\omega^{0.5}}$$

$$B = 0.2nF(D_0)^{2/3}\nu^{-1/6}C_0$$

where j is the current density, j_k is the kinetic current density, ω is the electrode rotation speed, n is the transferred

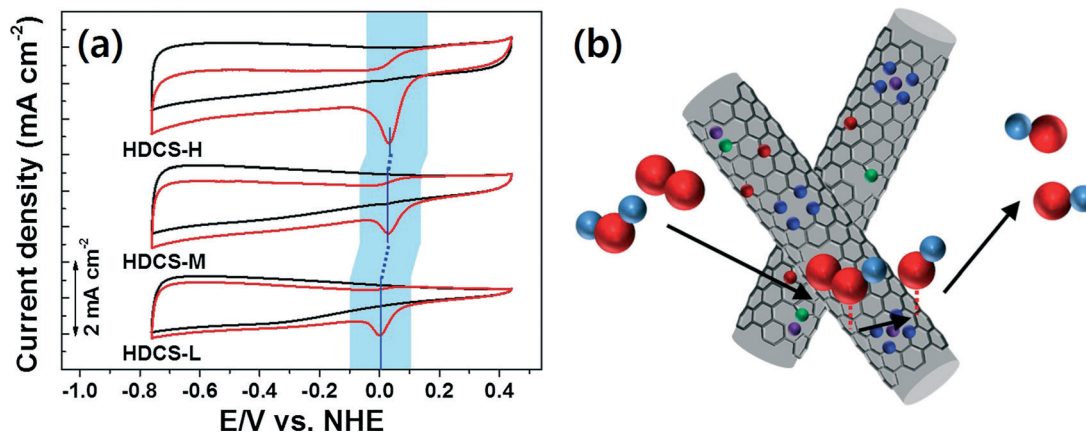


Fig. 3 (a) CVs of the as-prepared HDCS electrocatalysts in Ar- (black) and O₂- (red) saturated 1.0 M KOH electrolytes. (b) Schematic illustration of the reaction process of ORR in an alkaline electrolyte.

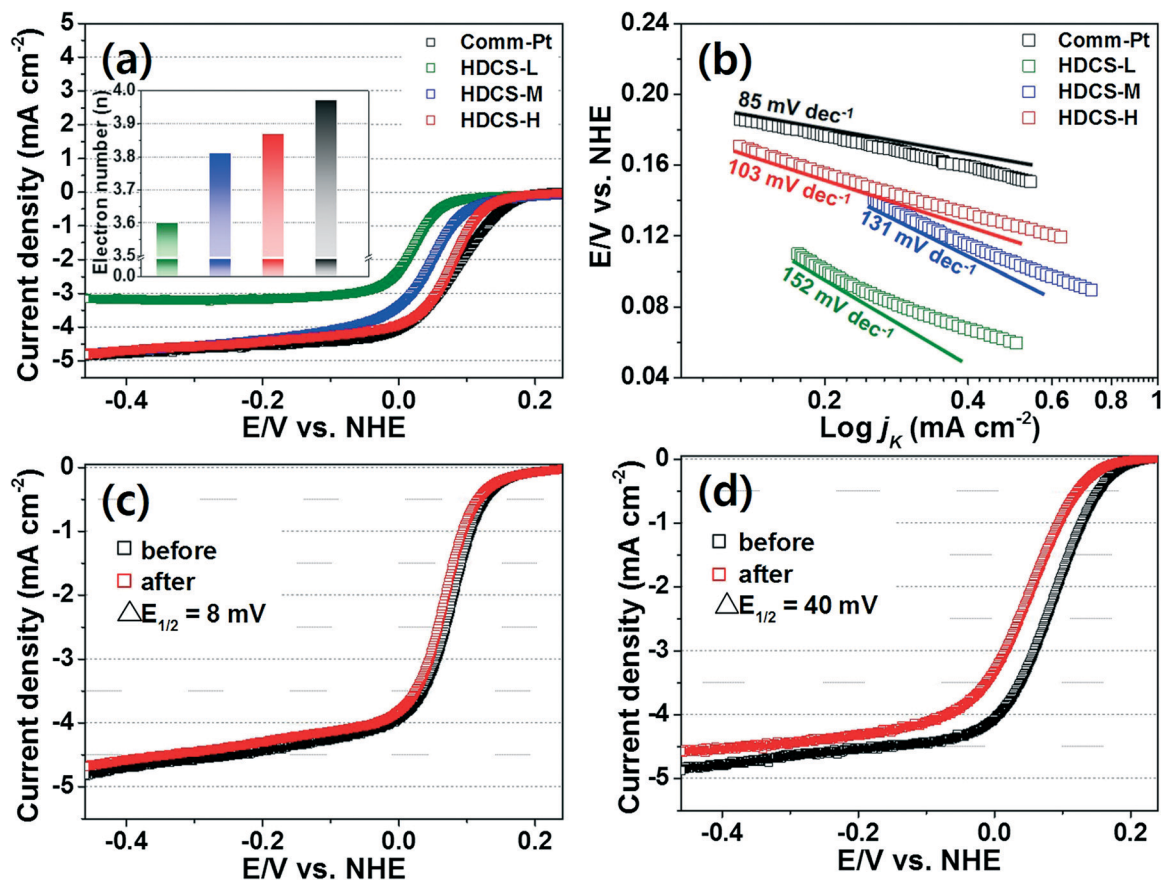


Fig. 4 (a) LSVs of the HDCS and commercial Pt electrocatalysts in O_2 -saturated 1.0 M KOH [the inset indicates the numbers of exchanged electrons of all as-prepared electrocatalysts]. (b) Tafel plots of the HDCS and commercial Pt electrocatalysts. Comparison of LSVs before and after the stability tests of (c) HDCS-H and (d) commercial Pt electrocatalysts.

electron number per oxygen molecule, F is the Faraday constant, D_0 is the diffusion coefficient of O_2 , ν is the kinematic viscosity of the electrolyte and C_0 is the bulk O_2 concentration. Very significantly, the transferred electron number of HDCS-H of the ORR obtained from the Koutecky–Levich plots (Fig. S4†) was ~ 3.87 , indicating definitely four electron transfer processes. Moreover, electron transfer numbers of 3.81 and 3.60 were obtained for HDCS-M and HDCS-L, respectively, suggesting nearly four electron transfer processes. In addition, it was also found that the HDCS-H electrocatalyst exhibits a relatively low Tafel slope of 103 mV dec^{-1} , indicating the enhanced catalytic activity with low overpotentials as well as the fast electron transfer kinetics, as shown in Fig. 4(b). In order to further address the effect of dopants in the HDCSs on the ORR activity, we performed LSV measurements with undoped, N-doped, Co–N-doped and Fe–N-doped carbon structures (denoted as only CS, N-DCS, Co-DCS and Fe-DCS, respectively) as shown in Fig. S5.† As expected, the HDCS exhibited superior electrochemical activities in ORR, *i.e.*, more positive half-wave potential, high current density at 0.04 V and fast on-set potential, compared to only CS, N-DCS, Co-DCS and Fe-DCS, because of their synergistic effect associated with the presence of the well-incorporated Fe and Co sites in the carbon structures as active sites (see more

detailed discussion in the ESI† (Fig. S5)). In particular, it has been reported that the coexistence of incorporated Fe and Co adatoms bound with N can reduce the binding energy of oxygen molecules on a non-precious metal electrocatalyst and hence can engineer electronic structures, for example, down-shifting of the d-band center, compared to individual Fe–N or Co–N bonding, resulting in the enhancement of ORR activities.²⁵ Furthermore, Wang's group recently demonstrated that hybrid N-modified transition metal sites can act as quite superior active sites for ORR because of their unique electrical and chemical properties, *i.e.*, the more positive charge of Fe induced by charge transfer from Fe to N, the strong OOH adsorption energy, and the strong chemical bonding between Fe and pyridine.^{45,46} Overall, these results suggest that the excellent electrochemical ORR activity of the HDCS-H electrocatalyst, such as the increased positive shift of ORR potentials, the electro-reduction reaction close to four electron transfer numbers, and low overpotential, is attributed to the relatively high contents of electrocatalytically active sites and their chemical structure associated with hybrid heterobimetal–N doping species, resulting from pyridinic–N and pyrrolic–N sites, which are energetically attractive to bind with transition metal atoms.^{47–49}

To evaluate the electrochemical stability of the optimized HDCS-H electrocatalyst, linear potential sweeps were carried out over 2000 cycles between -0.4 and $+0.1$ V (vs. Hg/HgO) using a scan rate of 50 mV s^{-1} in an O_2 -saturated 1.0 M KOH electrolyte. Fig. 4(c and d) show the ORR activities of the HDCS-H electrocatalyst measured between -0.6 and 0.1 V (vs. Hg/HgO) with a scan rate of 5 mV s^{-1} in O_2 -saturated 1.0 M KOH before and after the stability test. Remarkably, the HDCS-H electrocatalyst exhibited superior stability with a slight decrease of $\sim 8 \text{ mV}$ in half-wave potential, outperforming most precious metal catalysts reported previously, whereas the commercial Pt/C electrocatalyst exhibited a relatively significant decrease in half-wave potential ($\sim 40 \text{ mV}$). Thus, it is believed that our findings open up the possibility of new approaches to design and fabricate a variety of other non-precious metal electrocatalysts with excellent ORR activity and stability for practical applications in fuel cells.

Conclusions

In summary, we have prepared hybrid-doped 1-D functional carbon structures consisting of hetero-transition metallic iron and cobalt coordinated by pyridinic and pyrrolic nitrogen atoms, as electrocatalysts for ORRs, using a modified electrospinning technique. We have demonstrated that the HDCS-H electrocatalyst has a relatively high content of hybrid heterobimetal-nitrogen dopants synergistically incorporated into the carbon structures as active sites for ORRs. Therefore, these electrocatalysts show remarkably superior ORR electrocatalytic abilities *i.e.*, higher current density, more positive reduction potential, electron transfer number close to 4 and excellent electrochemical stability, comparable to previously reported other non-precious metal electrocatalysts and commercial Pt/C electrocatalysts. Thus, it is expected that the as-prepared HDCS-H electrocatalyst can be utilized as a promising non-precious metal cathode electrocatalyst in fuel cell applications.

Experimental

Fabrication of hybrid metal-nitrogen-doped functional carbon structures (HDCSs)

The precursor solution was prepared by dissolving 10 wt\% precursors with mixed polyacrylonitrile (PAN, $(\text{C}_3\text{H}_3\text{N})_m$, $M_w = 150\,000 \text{ g mol}^{-1}$, Aldrich) and metal-phthalocyanine (M-Pc) in *N,N*-dimethylformamide (DMF, $\text{HCON}(\text{CH}_3)_2$, Aldrich) solvent. In order to control the doping amount of metal and nitrogen, the ratios between PAN, iron phthalocyanine (Fe-Pc) and cobalt phthalocyanine (Co-Pc) in the precursor solution for the electrospinning process were controlled from $9.9:0.05:0.05$, $9.5:0.25:0.25$ and $9.0:0.5:0.5$, respectively. The precursor solution was loaded into a plastic syringe connected to a blunt-tip needle, which was connected to a syringe pump. The distance between the tip and Al collector was 15 cm . The electrospinning process was then carried out using a high

voltage (15 kV) linked to the needle tip of a syringe offering the well-prepared solution at a flow rate of $10 \mu\text{L min}^{-1}$. The electrospun fibers were dried in an oven at $60 \text{ }^\circ\text{C}$ for 24 h and then carbonized in a tube furnace at $900 \text{ }^\circ\text{C}$ for 3 h under a nitrogen atmosphere with a heating rate of $10 \text{ }^\circ\text{C min}^{-1}$ in order to obtain the HDCS electrodes.

Structural and chemical analysis

The as-prepared samples were characterized by FE-SEM and EDX spectroscopy using a JSM-6700F (JEOL Ltd.) microscope operating at 5 kV and TEM using a Philips Tecnai F20 system operating at 200 kV . The crystal structure was studied by XRD (D2 PHASER, Bruker AXS) with a $\text{Cu K}\alpha$ ($\lambda = 0.15418 \text{ nm}$) source with a nickel filter. The source was operated at 30 kV and 10 mA . The 2θ angular scan from 10° to 80° was explored at a scan rate of $0.5^\circ \text{ min}^{-1}$. Also, XPS (Thermo VG, U.K.) analysis was carried out with an $\text{Al K}\alpha$ X-ray source of 1486.6 eV at a chamber pressure below $1 \times 10^{-8} \text{ Torr}$ and a beam power of 200 W . All high-resolution spectra were collected using a pass energy of 46.95 eV . The step size and time per step were set at 0.025 eV and 100 ms , respectively. The $\text{C } 1s$ electron binding energy was referenced at 284.6 eV and a nonlinear least-squares curve-fitting program was employed with a Gaussian-Lorentzian production function.

Electrochemical characterization in ORRs

The electrochemical properties of the as-prepared electrocatalysts in ORRs were measured in a three-electrode cell at $25 \text{ }^\circ\text{C}$ using a potentiostat (Eco Chemie, AUTOLAB). The as-prepared HDCS electrocatalyst inks were prepared by mixing the electrocatalyst, deionized water, isopropyl alcohol and 5 wt\% Nafion solution. The glassy carbon working electrode was coated with $0.5 \mu\text{L}$ of the electrocatalyst inks and dried in an oven at $50 \text{ }^\circ\text{C}$. The total loading of the electrocatalyst in all HDCS electrocatalysts was $400 \mu\text{g cm}^{-2}$. To compare the electrochemical properties, we used commercial Pt electrocatalysts, and the loading amount of the Pt electrocatalyst was $40 \mu\text{g cm}^{-2}$. In addition, a Pt wire and Ag/AgCl (in saturated 3 M KCl) were used as counter and reference electrodes, respectively. The cyclic voltammograms (CVs) of the electrocatalysts were obtained in Ar- or O_2 -saturated 1.0 M KOH with a scan rate of 50 mV s^{-1} at $25 \text{ }^\circ\text{C}$. The oxygen reduction current-potential curves were obtained using linear sweep voltammetry (LSV) at various rotation speeds from 100 to 2500 rpm in an O_2 -saturated 1.0 M KOH solution by sweeping the potential from -0.6 to 0.1 V at a scan rate of 5 mV s^{-1} . The stability test in ORRs was carried out by applying linear potential sweeps for 2000 cycles. The oxygen reduction current-potential curves after the stability test of the electrocatalysts were obtained by sweeping the potential from -0.6 to 0.1 V . All potentials were calibrated with respect to the normal hydrogen electrode (NHE).⁵⁰

Acknowledgements

This work was supported by the International Collaborative Energy Technology R&D Program of the Korea Institute of Energy Technology Evaluation and Planning (KETEP), granted financial resource from the Ministry of Trade, Industry & Energy (No. 20138520030800) and Basic Science Research Program through the National Research Foundation of Korea (NRF) funded by the Ministry of Education (No. 2015R1A6A3A03019704), Republic of Korea.

References

- 1 A. Kraytsberg and Y. Ein-Eli, *Energy Fuels*, 2014, **28**, 7303–7330.
- 2 R. Devandathan, *Energy Environ. Sci.*, 2008, **1**, 101–119.
- 3 S. J. Peighambaroust, S. Rowshanzamir and M. Ajadi, *Int. J. Hydrogen Energy*, 2010, **35**, 9349–9384.
- 4 J. Larminie and A. Dicks, *Fuel Cell Systems Explained*, John Wiley & Sons Ltd, West Sussex, 2nd edn., 2003.
- 5 Y. Wang, K. S. Chen, J. Mishler, S. C. Cho and X. C. Adroher, *Appl. Energy*, 2011, **88**, 981–1007.
- 6 Y.-W. Lee, S. N. Cha, K.-W. Park, J. I. Sohn and J. M. Kim, *J. Nanomater.*, 2015, **2015**, 273720.
- 7 M. Wang, W. Zhang, J. Wang, A. Minett, V. Lo, H. Liu and J. Chen, *J. Mater. Chem. A*, 2013, **1**, 2391–2394.
- 8 S. Ghosh, S. Mondal and C. R. Raj, *J. Mater. Chem. A*, 2014, **2**, 2233–2239.
- 9 Y. Zhai, X. Xu and Y. Jin, *Adv. Mater.*, 2012, **24**, 1594–1597.
- 10 S. J. Yoo, H.-Y. Park, T.-Y. Jeon, I.-S. Park, Y.-H. Cho and Y.-E. Sung, *Angew. Chem., Int. Ed.*, 2008, **47**, 9307–9310.
- 11 Y. Bing, H. Liu, L. Zhang, D. Ghosh and J. Zhang, *Chem. Soc. Rev.*, 2010, **39**, 2184–2202.
- 12 H. A. Gasteiger, S. S. Kocha, B. Sompalli and F. T. Wagner, *Appl. Catal., B*, 2005, **56**, 9–35.
- 13 M. K. Debe, *Nature*, 2012, **486**, 43–51.
- 14 H. T. Chung, J. H. Won and P. Zelenyay, *Nat. Commun.*, 2013, **4**, 1922.
- 15 A.-R. Ko, Y.-W. Lee, J.-S. Moon, S.-B. Han, G. Cao and K.-W. Park, *Appl. Catal., A*, 2014, **477**, 102–108.
- 16 C. W. B. Bezerra, L. Zhang, K. Lee, H. Liu, A. L. B. Marques, E. P. Marques, H. Wang and J. Zhang, *Electrochim. Acta*, 2008, **53**, 4937–4951.
- 17 G. Liu, X. Li, J.-W. Lee and B. N. Popov, *Catal. Sci. Technol.*, 2011, **1**, 207–217.
- 18 J.-S. Lee, K. Jo, T. Lee, T. Yun, J. Cho and B.-S. Kim, *J. Mater. Chem. A*, 2013, **1**, 9603–9607.
- 19 J. Zho, C. He, Y. Li, S. Kang and P. K. Shen, *J. Mater. Chem. A*, 2013, **1**, 14700–14705.
- 20 S. Wang, D. Yu, L. Dai, D. W. Chang and J.-B. Baek, *ACS Nano*, 2011, **5**, 6202–6209.
- 21 S. Maldonado and K. J. Stevenson, *J. Phys. Chem. B*, 2005, **109**, 4707–4716.
- 22 R. Liu, D. Wu, X. Feng and K. Müllen, *Angew. Chem., Int. Ed.*, 2010, **49**, 2565–2569.
- 23 G. Wu, K. L. More, C. M. Johnston and P. Zelenay, *Science*, 2011, **332**, 443–447.
- 24 S. Gong, F. Du, Z. Xia, M. Durstock and L. Dai, *Science*, 2009, **323**, 760–764.
- 25 J. Y. Cheon, T. Kim, Y. M. Choi, H. Y. Jeong, M. G. Kim, Y. J. Sa, J. Kim, Z. Lee, T.-H. Yang, K. Kwon, O. Terasaki, G.-G. Park, R. R. Adzic and S. H. Joo, *Sci. Rep.*, 2013, **3**, 2715.
- 26 Y. Hou, Z. Wen, S. Cui, S. Ci, S. Mao and J. Chen, *Adv. Funct. Mater.*, 2015, **25**, 872–882.
- 27 A. Sarapuu, L. Samolberg, K. Kreek, M. Koel, L. Matisen and K. Tammevesk, *J. Electroanal. Chem.*, 2015, **746**, 9–17.
- 28 J.-S. Moon, Y.-W. Lee, S.-B. Han, D.-H. Kwak, K.-H. Lee, A.-R. Park, J. I. Sohn, S. N. Cha and K.-W. Park, *Phys. Chem. Chem. Phys.*, 2014, **16**, 14644–14650.
- 29 R. Liu, D. Wu, X. Feng and K. Müllen, *Angew. Chem., Int. Ed.*, 2010, **49**, 2565–2569.
- 30 X.-H. Yan and B.-Q. Xu, *J. Mater. Chem. A*, 2014, **2**, 8617–8622.
- 31 L. Wu, H. Feng, M. Liu, K. Zhang and J. Li, *Nanoscale*, 2013, **5**, 10839–10843.
- 32 C.-H. Hsu, J.-Y. Jan, H.-P. Lin and P.-L. Kuo, *New J. Chem.*, 2014, **38**, 5521–5526.
- 33 J. Zhang, D. He, H. Su, X. Chen, M. Pan and S. Mu, *J. Mater. Chem. A*, 2014, **2**, 1242–1246.
- 34 K. Parvez, S. Yang, Y. Hernandez, A. Winter, A. Turchanin, X. Feng and K. Müllen, *ACS Nano*, 2012, **6**, 9541–9550.
- 35 M. Li, X. Bo, Y. Zhang, C. Han, A. Nsabimana and L. Guo, *J. Mater. Chem. A*, 2014, **2**, 11672–11682.
- 36 B. Zheng, J. Wang, F.-B. Wang and X.-H. Xia, *J. Mater. Chem. A*, 2014, **2**, 9079–9084.
- 37 X. Fu, J. Jin, Y. Liu, Q. Liu, K. Niu, J. Zhang and X. Cao, *Electrochem. Commun.*, 2013, **28**, 5–8.
- 38 M. Li, X. Bo, Y. Zhang, C. Han, A. Nsabimana and L. Guo, *J. Mater. Chem. A*, 2014, **2**, 11672–11682.
- 39 Y. Jiang, Y. Lu, X. Wang, Y. Bao, W. Chen and L. Niu, *Nanoscale*, 2014, **6**, 15066–15072.
- 40 Q. Dong, X. Zhuang, Z. Li, B. Li, B. Fang, C. Yang, H. Xie, F. Zhang and X. Feng, *J. Mater. Chem. A*, 2015, **3**, 7767–7772.
- 41 H. Peng, Z. Mo, S. Liao, H. Liang, L. Yang, F. Luo, H. Song, Y. Zhong and B. Zhang, *Sci. Rep.*, 2013, **3**, 1765.
- 42 T. Hu, S. Sun, H. Sun, G. Xin, D. Shao, C. Liu and J. Lian, *Phys. Chem. Chem. Phys.*, 2014, **16**, 1060–1066.
- 43 L. Wang, P. Yu, L. Zhao, C. Tian, D. Zhao, W. Zhou, J. Yin, R. Wang and H. Fu, *Sci. Rep.*, 2014, **4**, 5184.
- 44 H. Wang, K. Wang, J. Key, S. Ji, V. Linkov and R. Wang, *J. Electrochem. Soc.*, 2014, **161**, H637–H642.
- 45 X. Zhong, L. Liu, X. Wang, H. Yu, G. Zhuang, D. Mei, X. Li and J.-G. Wang, *J. Mater. Chem. A*, 2014, **2**, 6703–6707.
- 46 X. Zhong, H. Yu, G. Zhuang, Q. Li, X. Wang, Y. Zhu, L. Liu, X. Li, M. Dong and J.-G. Wang, *J. Mater. Chem. A*, 2014, **2**, 897–901.
- 47 S. M. Unni, S. Devulapally, N. Karjule and S. Kurunqot, *J. Mater. Chem.*, 2012, **22**, 23506–23513.
- 48 L. Feng, Y. Yan, Y. Chen and L. Wang, *Energy Environ. Sci.*, 2011, **4**, 1892–1899.
- 49 S. M. Unni, S. N. Bhande, R. Illathvalappil, N. Mutneja, K. R. Patil and S. Kurunqot, *Small*, 2015, **11**, 352–360.
- 50 L. Mattarozzi, S. Cattarin, N. Comisso, P. Guerriero, M. Musiani, L. Vázquez-Gómez and E. Verlato, *Electrochim. Acta*, 2013, **89**, 488–496.